LETTERS

# Contribution of anthropogenic and natural sources to atmospheric methane variability

P. Bousquet[1,2], P. Ciais[1], J. B. Miller[3,4], E. J. Dlugokencky[3], D. A. Hauglustaine[1], C. Prigent[5], G. R. Van der Werf[6], P. Peylin[7], E.-G. Brunke[8], C. Carouge[1], R. L. Langenfelds[9], J. Lathière[1], F. Papa[5,10], M. Ramonet[1], M. Schmidt[1], L. P. Steele[9], S. C. Tyler[11] & J. White[12]

**Methane is an important greenhouse gas, and its atmospheric concentration has nearly tripled since pre-industrial times[1]. The growth rate of atmospheric methane is determined by the balance between surface emissions and photochemical destruction by the hydroxyl radical, the major atmospheric oxidant. Remarkably, this growth rate has decreased[2] markedly since the early 1990s, and the level of methane has remained relatively constant since 1999, leading to a downward revision of its projected influence on global temperatures. Large fluctuations in the growth rate of atmospheric methane are also observed from one year to the next[2], but their causes remain uncertain[2–13]. Here we quantify the processes that controlled variations in methane emissions between 1984 and 2003 using an inversion model of atmospheric transport and chemistry. Our results indicate that wetland emissions dominated the inter-annual variability of methane sources, whereas fire emissions played a smaller role, except during the 1997–1998 El Niño event. These top-down estimates of changes in wetland and fire emissions are in good agreement with independent estimates based on remote sensing information and biogeochemical models. On longer timescales, our results show that the decrease in atmospheric methane growth during the 1990s was caused by a decline in anthropogenic emissions. Since 1999, however, they indicate that anthropogenic emissions of methane have risen again. The effect of this increase on the growth rate of atmospheric methane has been masked by a coincident decrease in wetland emissions, but atmospheric methane levels may increase in the near future if wetland emissions return to their mean 1990s levels.**

The global growth rate of atmospheric methane ($CH_4$) decreased from nearly $+12 \pm 2$ p.p.b. $yr^{-1}$ in the 1980s to $+4 \pm 4$ p.p.b. $yr^{-1}$ in the last decade (all values are means $\pm$ s.d.), but with large year-to-year variations[2] (Fig. 1a). A peak in growth rate occurred in 1991 in the tropics, followed by a large and abrupt drop in 1992, which began in the northern regions. The past few years have been marked by two positive growth-rate anomalies in 1997–1998 and in 2002–2003, which seem more pronounced north of 30 °N than in the tropics.

To understand better why the growth rate of $CH_4$ has remained persistently smaller after the early 1990s, we have analysed the regional trends in $CH_4$ differences between sampling sites in the National Oceanic and Atmospheric Association (NOAA) global co-operative air sampling network[2] and the South Pole site, taken as a reference (Fig. 1b and Supplementary Information). This analysis suggests that either northern $CH_4$ emissions have declined persistently since 1992 or that the destruction of $CH_4$ by the hydroxyl radical (OH) has increased north of 30 °N. Several conflicting hypotheses have been proposed to explain interannual and long-term variations in atmospheric $CH_4$, focusing on wetland $CH_4$ emissions[10,13,14], anthropogenic $CH_4$ emissions[5], wild fires[6–9,15], OH photochemistry[3,4,11] and inter-annual wind changes[12]. Various models have been used, but the contribution of each process has not been disentangled in a coherent framework, except for short periods[6,16]. Our understanding of the current methane budget therefore remains plagued by very large uncertainties.

Atmospheric $CH_4$ measurements can be linked quantitatively to regional sources and sinks by inverse modelling. For the period 1984–2003, the $CH_4$ concentration responses to the action of OH sinks and regional surface sources were simulated each month with the three-dimensional chemistry transport model LMDZ-INCA[17]. The model was forced with interannual analysed winds[18] and inter-annually varying OH concentrations[19]. Emissions of $CH_4$ from different regions of the globe and from distinct processes (see Methods), together with the photochemical sinks, were inferred, and their uncertainties reduced, by matching atmospheric observations within their uncertainties in a bayesian formalism[19]. Clearly, uncertainties in the variations of OH concentrations limit our ability to infer accurately fluctuations in regional $CH_4$ emissions. The removal of $CH_4$ by OH nearly balances the sum of all surface sources, making the atmospheric $CH_4$ budget highly sensitive to OH changes. Thus, we constrained first the interannual variability of OH through a preliminary inversion of methyl chloroform atmospheric observations[19]. Contributions of monthly surface $CH_4$ sources and pre-optimized monthly OH sinks were then combined to fit optimally monthly averages of $CH_4$ measurements from a global network of 68 sampling sites. Long-term measurements of the $^{13}C/^{12}C$ ratio in $CH_4$ ($\delta^{13}C\text{-}CH_4$) were also used as an additional constraint for the partitioning of microbial-, biomass-burning- and fossil-fuel-related $CH_4$ sources. We performed a control inversion, supplemented by an ensemble of 17 sensitivity inversions (see Methods).

We found that the year-to-year $CH_4$ regional flux changes (or anomalies) can be more robustly inverted than their mean values, a result similar to $CO_2$ inversions[20,21]. Indeed, among the different sensitivity inversions, the spread of regional flux anomalies is more than a factor of two smaller than the spread of long-term mean fluxes. In other words, possible biases in the inversions seem to have low interannual variability. To illustrate this point, we tested the impact

[1]Laboratoire des Sciences du Climat et de l'Environnement, IPSL-LSCE, CEA-CNRS-UVSQ, F-91191, France. [2]Université de Versailles Saint Quentin en Yvelines, F-78035, France. [3]NOAA Earth System Research Laboratory, Global Monitoring Division, Boulder, Colorado 80305-3328, USA. [4]Cooperative Institute for Research in Environmental Science, Campus Box 216, University of Colorado, Boulder, Colorado 80309, USA. [5]LERMA, Observatoire de Paris, F-75014, France. [6]Faculty of Earth and Life Sciences, Vrije Universiteit, Amsterdam, The Netherlands. [7]Laboratoire de Biogéochimie Isotopique, LBI, F-78026, France. [8]South African Weather Service, Stellenbosch 7599, South Africa. [9]CSIRO, Marine and Atmospheric Research, Victoria 3195, Australia. [10]NASA-GISS-Columbia University, New York, New York 10025, USA. [11]Earth System Science Department, University of California, Irvine, California 92697, USA. [12]Institute of Arctic and Alpine Research, University of Colorado, Boulder, Colorado 80309, USA.

of adding an additional methane source from plants[22] with an *a priori* value of $+150 \pm 60 \times 10^{12}$ grams of $CH_4$ per year (Tg of $CH_4$ $yr^{-1}$). The long-term-mean inverted fluxes were strongly affected by this 'intrusion' of this new source, but the atmospheric measurements remained fitted and the global budget was conserved, after a reduction in plant and other source emissions (−30%) within their uncertainties. The sparseness of the tropical network, along with large uncertainties on prior emissions, prevents us from verifying the existence of long-term $CH_4$ emissions by plants. Adding plants in the *a priori* $CH_4$ sources mix, however, did not alter the inferred anomalies in the 1990s (see Supplementary Information). Given their robustness, the flux anomalies are therefore the primary focus of the following analysis.

We found that fluctuations in wetland emissions are the dominant contribution to interannual variability in surface emissions (±12 Tg of $CH_4$ $yr^{-1}$), explaining 70% of the global emission anomalies over the past two decades, as compared with only 15% contributed by biomass burning (Fig. 2). This result disagrees with previous studies suggesting a dominant role of fires[6–9,14]. As an independent check on the inverted wetland variability, we applied a simple wetland flux model (see Supplementary Information) based on ref. 23 and driven by interannually varying climate data[18] and by estimates of remotely sensed changes in flooded areas for the period 1993–2001. There is good agreement in the magnitude of the wetland flux anomalies between the bottom-up and inversion results (normalized standard deviation (NSD) = 1.1; see Methods), as seen in Fig. 2. The correlation between the two estimates is improved when a 3-month lag is applied to the inversion results ($r^2 = 0.4$, $P = 0.06$). In 1993–2001, wetland emissions in the bottom-up model show a persistent negative trend of 2.5 Tg of $CH_4$ $yr^{-1}$, in response to a marked decrease in flooded area worldwide (at a rate of $-1.1\%$ $yr^{-1}$ for a mean area of $4.2 \times 10^6$ $km^2$), mostly in temperate and tropical Asia and in tropical South America[23]. The inversion infers decreasing wetland emissions after 1993, but with a smaller trend (−0.6 Tg of $CH_4$ $yr^{-1}$). Shrinking wetland areas may reflect recurrent dryness observed in the tropics after 1990 (ref. 18), and northward after 1999 (ref. 24).

The inversion attributes global variations in the biomass-burning emissions of the order of ±3.5 Tg of $CH_4$ $yr^{-1}$ (Fig. 2). In 1989–2002, these anomalies are in very good agreement with independent estimates[9] derived from remote sensing data after 1996 ($r^2 = 0.6$, $P = 0.012$; NSD = 0.8) and inferred from global CO variations before 1996 ($r^2 = 0.4$, $P = 0.08$; NSD = 1.2; see Supplementary Information). Such agreement is remarkable, given that the *a priori* biomass-burning fluxes prescribed to the inversion are constant from year to year. The members of the inversion ensemble that include $\delta^{13}C$-$CH_4$ observations agree best with the magnitude of the bottom-up anomalies[9] (NSD = 1.1). At face value, these 'isotopic' inversions

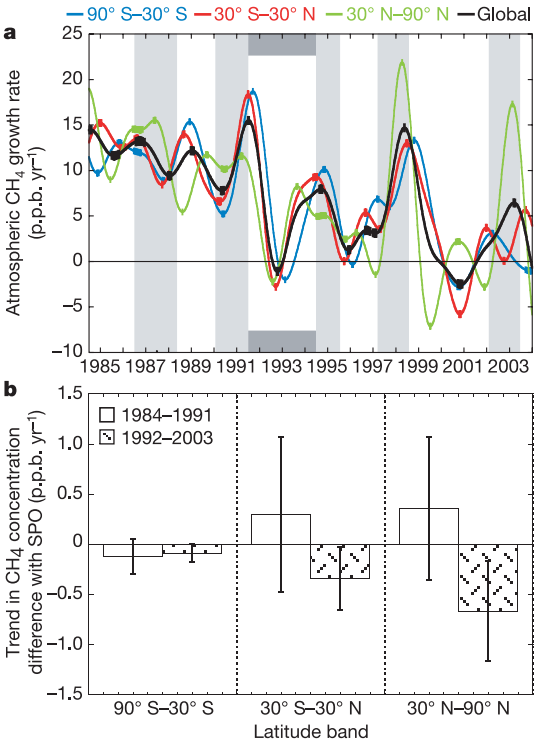


**Figure 1 | Variability and trends in atmospheric $CH_4$ over the past two decades.** **a**, Interannual variations in the growth rate of atmospheric $CH_4$ (p.p.b. $yr^{-1}$) in the period 1984–2003, calculated by using data from the NOAA air sampling sites used in the inversion model (maximum of 50 sites). Black, global growth rate; blue, Southern Hemisphere <30 °S; red, 30 °S to 30 °N (tropics); green, Northern Hemisphere >30 °N; light grey, El Niño episodes; dark grey, anomaly following the Pinatubo climate anomaly. **b**, Average trends in the $CH_4$ difference (in p.p.b. $yr^{-1}$) between sites grouped in three latitude bands and the South Pole site (SPO). Trends were calculated by using monthly deseasonalized observations. Open bars indicate trends in $\Delta CH_4$ in the 1980s (1984–1991), when the global growth rate was $+12 \pm 2$ p.p.b. $yr^{-1}$; hatched bars indicate trends in $\Delta CH_4$ after 1993, when the global growth rate was $4 \pm 4$ p.p.b. $yr^{-1}$. Error bars are 1 s.d. of the calculated trends in differences for the NOAA sites.

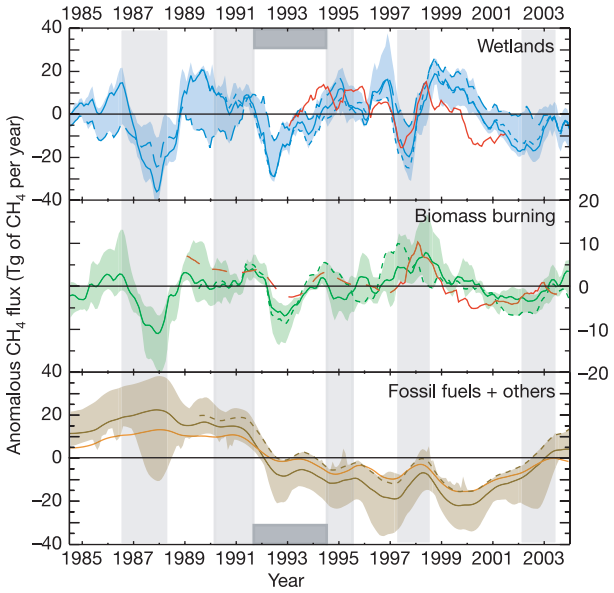


**Figure 2 | Variations in $CH_4$ emissions attributed to different processes.** Shown are the interannual global $CH_4$ flux anomalies (in Tg of $CH_4$ $yr^{-1}$; note different *y*-axis scales) broken down into different processes. Unbroken lines of each sub-panel indicate the member of the ensemble with only $CH_4$ observations (control inversion, 68 sites); broken lines of each sub-panel indicate the member of the ensemble with both $CH_4$ observations (68 sites) and $\delta^{13}C$-$CH_4$ observations (13 sites after 1998; 4 sites after 1989). Blue indicates wetlands (including rice agriculture); dashed blue line represents wetland anomaly inferred in the extreme case where OH is maintained constant from year to year. Green indicates biomass burning. Brown indicates energy-related sources (fossil fuels, industry, bio-fuels) and other sources (landfills and waste, ruminants, termites, ocean, plants). Unbroken orange line represents the specific contribution of fossil-fuel emissions alone. Red lines indicate set of bottom-up estimates of $CH_4$ flux anomalies obtained from a wetland flux model driven by remotely sensed flooded area data[22], and from a fire model driven by remote sensing measurements after 1997 (ref. 9), and extrapolated using atmospheric carbon monoxide trends before that date (see Supplementary Information). The anomalies are calculated by subtracting the long-term mean $CH_4$ flux over the whole period (1984–2003) from the deseasonalized (12-month running mean) monthly flux in each region. Shaded areas represent the spread of an ensemble of 18 inversions (each using *a priori* OH fields pre-optimized from methyl chloroform).

place a strong (tropical) release of $CH_4$ by fires in 1997, six months earlier than inferred from the remote sensing data (Fig. 2).

The regional patterns of surface $CH_4$ emissions indicate that most of the global year-to-year variability lies in the tropics (Fig. 3). By contrast, the northern regions show smoother variations, but with systematically less emissions in the 1990s than in the 1980s, except for 1997–1998 and 2002–2003, consistent with Fig. 1b. The variability in $CH_4$ removal by OH radicals[19] is also dominated by the tropics, where photochemistry remains active all year (Fig. 3). We found that the years 1987–1988, 1991–1992, 1997–1998 and 2001–2002 correspond to abnormally weaker $CH_4$ destruction by OH in the tropics. In the inversion, a compensation effect exists between the magnitude of methyl-chloroform-derived changes in OH and inverted $CH_4$ surface emissions, because the sum of the two must equal the observed atmospheric accumulation. Thus, biases in OH changes could account for some of the variability that we attributed to wetlands. In the extreme case where OH interannual variability is set at zero, the fluctuations of tropical wetland emissions are dampened by 50%, especially in the 1980s, when methyl chloroform data suggest large OH variability[19].

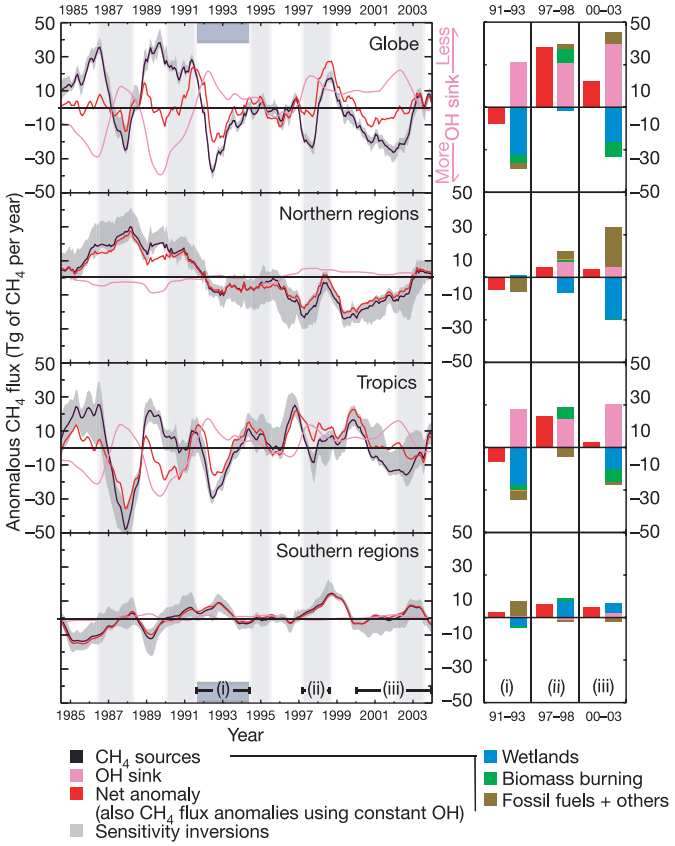


**Figure 3 | Large-scale regional variations in $CH_4$ emissions and OH sink.** Left, interannual flux anomalies (in Tg of $CH_4$ $yr^{-1}$) broken down into three large regions[27] for the control inversion: northern regions, tropics and southern regions. Black indicates surface emission anomaly, with grey uncertainty estimates based on the spread of the ensemble of 18 inversions (each using *a priori* OH variations pre-optimized from methyl chloroform). Pink indicates anomalies in $CH_4$ removal by OH (negative values mean more $CH_4$ removal). Red indicates anomalies in the net $CH_4$ budget in each band; that is, the sum of surface emissions and OH removal. This red line also represents what the surface emissions anomalies would be in the extreme case where OH is maintained constant from year to year. Right, changes in surface emissions and in the OH removal term within each large region during selected remarkable episodes analysed in the text: the drop in $CH_4$ growth rate of 1991–1993; the high $CH_4$ growth rate of the 1997–1998 largest El Niño event; and the persistent low mean atmospheric growth rate of 2000–2003. The 1991–1993 anomaly is discussed after subtraction of the mean flux over 1984–2003. The 1997–1998 and the 2000–2003 anomalies are discussed after subtraction of the mean flux over 1993–2003. Quantities refer to the full episode (Tg of $CH_4$). Each source is coloured as in Fig. 2. A positive bar indicates an increase in surface emission and a decrease in OH removal.

We analysed in detail two key perturbations of the $CH_4$ budget in the past two decades (Fig. 3). First, we studied the drop in growth rate in 1991–1993. This period is particularly intriguing because of the potentially confounding effects of three factors: (1) reduced photochemical production caused by changes in ultraviolet radiation associated with volcanic aerosols emitted in the eruption of the Mount Pinatubo in June 1991; (2) the widespread Northern Hemisphere cooling that followed[25]; and (3) the economic collapse of the former Soviet Union. The first factor should decrease OH, causing $CH_4$ to increase. Indeed, we inferred a decrease in tropical OH by 5% from the methyl chloroform data[19], as suggested by Fig. 1b and previous studies[4]. The two other factors should reduce wetland and fossil-fuel emissions respectively, causing atmospheric $CH_4$ to decrease. Overall, we attribute the 1991–1993 spike in growth rate, a $-10$ Tg of $CH_4$ event (Fig. 3), to a large decrease in emissions ($-36 \pm 6$ Tg of $CH_4$) partly offset by a reduction in the OH sink intensity ($+26$ Tg of $CH_4$). Sources that were reduced in that period are predominantly northern and tropical wetlands ($-24 \pm 6$ Tg of $CH_4$) and anthropogenic sources ($-10 \pm 5$ Tg of $CH_4$). Decreased biomass-burning emissions had a much smaller role ($-5 \pm 2$ Tg of $CH_4$). This inversion result agrees well with an independent study showing reduced boreal wetland emissions due to cooler and dryer conditions[10], and reduced northern anthropogenic emissions[26].

Second, we investigated the period 1997–1998, which corresponds to the largest El Niño on record. At that time, widespread dryness caused increases of fires in the tropical zone and in boreal regions of Eurasia[9]. In particular, large abnormal peat fires in Indonesia could have released huge amounts of $CH_4$ to the atmosphere from smouldering combustion[15]. A previous study[9] estimated an anomalous fire source of $+11.5$ Tg of $CH_4$ in 1997–1998 (Fig. 3), which agrees well with the inversion estimates ($+8 \pm 2$ Tg of $CH_4$ in the tropics and $+2 \pm 1$ Tg of $CH_4$ in northern regions). A larger decrease in OH concentration, possibly also caused by large emissions of carbon monoxide[16] and other reactive carbon compounds by fires[7], is found to contribute to a faster growth of $CH_4$ by an additional $+26$ Tg of $CH_4$. Natural wetland emissions remained on average stable over the whole 1997–1998 period. However, there was a significant dip in 1997 for the northern regions wetlands ($-9 \pm 5$ Tg of $CH_4$), followed by an increase in 1998 ($+10 \pm 5$ Tg of $CH_4$) in the southern regions (Fig. 3). This shift in regional wetland emissions is fully consistent with the succession of regionally dryer and wetter climate conditions[18].

Finally, we analysed why the global growth rate of atmospheric $CH_4$ remained low after the drop in 1991–1993 (ref. 4). After 1993, decreasing global emissions at a rate of $-1.0 \pm 0.2$ Tg of $CH_4$ $yr^{-1}$ are required to match a small average growth rate of $+4 \pm 4$ p.p.b. $yr^{-1}$, in the presence of (slightly) decreasing OH (Fig. 3). The inversion attributes this signal to decreasing anthropogenic emissions, in particular to the northern fossil source (Fig. 3). This is in qualitative agreement with the latitudinal $CH_4$ differences analysed in Fig. 1b. After 1999, however, anthropogenic emissions increase again, especially in north Asia. This may reflect the booming Chinese economy. By 2003, we find that anthropogenic emissions recovered to their levels in the early 1990s. Without a coincident and important drop in northern wetland emissions after 1999 (Fig. 2) associated with dryer conditions[24], the growth rate of atmospheric $CH_4$ would therefore have increased much more rapidly. This suggests that the slow-down in $CH_4$ growth rate observed from the early 1990s may represent only a temporary pause in the human-induced secular increase in atmospheric $CH_4$.

Better knowledge of the current $CH_4$ budget helps to reduce uncertainties in future projections of climate change and tropospheric

ozone evolution and to design effective mitigation strategies. Atmospheric long-term measurements and inverse models currently provide key information for assessing $CH_4$ emission trends at the global to subcontinental scale. Given uncertainties in surface emissions and OH distribution, however, using this approach at the regional or country scale remains challenging and requires an observational network that is dense in space and time[27]. In the future, the combined use of improved emission inventories, isotopic observations and global space-borne measurements of column-integrated $CH_4$ should help better to quantify regional sources, to separate natural from anthropogenic processes, and to verify the effectiveness of $CH_4$ mitigation policies.

## METHODS

**Inversion model setup.** The inverse methodology has been fully described[19] through the example of OH field optimization against methyl chloroform observations. For $CH_4$, surface emissions are optimized each month for 11 land regions (those defined in ref. 28), one global ocean region, and up to ten processes over each land region (emissions from bogs, swamps, tundra, termites, fossil fuel and industry, gas, bio-fuel, ruminant animals, landfills and waste, and soil uptake). This spatial partition enables us to perform both geographically based and process-based analyses. On a geographical basis, the optimized emissions were further aggregated, after inversion, over three large regions: northern regions (boreal & temperate North America, boreal & temperate Asia, and Europe, roughly $>30\,^{\circ}$N), tropical regions (tropical America, north and South Africa, tropical Asia), and southern regions (temperate South America and Oceania, roughly $<30\,^{\circ}$S). We used the optimized interannual four-dimensional distribution of OH from ref. 19. The variations in OH are pre-optimized from methyl chloroform data using interannual winds and chemistry (see Supplementary Information). In this procedure, the inferred interannual OH fields also depend on methyl chloroform sources. Uptake of $CH_4$ by soils is optimized as an independent sink, but we do not explicitly solve for the stratospheric sink of $CH_4$ but assume that it is included in the removal by the stratospheric OH radicals of the INCA model[17].

Atmospheric $CH_4$ observations, from roughly weekly air samples collected in flasks, were inverted as monthly means. Uncertainties in the monthly means were taken from the GLOBALVIEW-$CH_4$ data product[29], when available, or from submonthly variability in the measurements. In total, data from 68 sites from different networks were collected and used; 75% was contributed by the NOAA network. Offsets between different observing networks were accounted for by using intercomparison round-robin information reported in GLOBALVIEW-$CH_4$. The sampling periods for each site, and data uncertainties, are given in Supplementary Table A2. Atmospheric $\delta^{13}$C-$CH_4$ flask data from 13 NOAA sites were used in the inversion for the 1998–2004 period (Supplementary Table A2). The $\delta^{13}$C-$CH_4$ values were measured by INSTAAR at the University of Colorado[30]. At four sites (Point Barrow, Mauna Loa, Samoa and South Pole), the NOAA observations were merged with those from the SIL network[31] to extend the time series for the period 1989–2004. The gap in $\delta^{13}$C-$CH_4$ data in the period with no observations in 1996–1997 was filled by interpolation, and the interpolated values associated with a large *a priori* uncertainty in the inversion. At Niwot Ridge, the UCI network time-series[32] was used to extend the atmospheric $\delta^{13}$C-$CH_4$ record back to 1994. Although isotopic ratios are monitored at only 13 sites, they are expected to constrain usefully the partitioning of $CH_4$ sources according to their mean isotopic signature: biomass burning (about $-20$‰ for C-3 plants; about $-12$‰ for C-4 plants), all bacterial processes (about $-60$‰) and fossil-fuel-related sources (about $-40$‰), the atmosphere being close to $-47$‰ on average. The carbon isotopes measurements are relative to Vienna Pee Dee Belemnite (VPDB).

The inversion of $CH_4$ fluxes accounts for the fact that $CH_4$ removal by OH radicals is a nonlinear function of surface $CH_4$ emissions, by iteratively applying the forward and the inverse transport chemistry model up until convergence is reached for the OH removal of $CH_4$. In inversions using $\delta^{13}$C-$CH_4$ data, we account for the fact that transport and chemistry of $\delta^{13}$C-$CH_4$ is nonlinear by solving iteratively for both the underlying $CH_4$ source magnitude and its isotopic composition, as in ref. 33.

**Sensitivity tests.** The settings of the inversion model that were varied in the sensitivity tests were (1) the *a priori* error on regional fluxes; (2) the *a priori* error on the atmospheric $CH_4$ and $\delta^{13}$C-$CH_4$ measurements; (3) the number of land regions to be optimized; (4) the size of the atmospheric network; (5) the use of non interannual transport; (6) the uses of non-interannual OH; (7) the introduction of an additional source due to possible $CH_4$ emission by plants[22]. See Supplementary Table A2 for a complete description of the 18 inversions performed.

**NSD.** The normalized standard deviation (NSD) is calculated as the ratio between the s.d. of the monthly deseasonalized inverted $CH_4$ flux anomaly and the s.d. of the same anomaly calculated by the bottom-up model. An NSD value of 1 indicates a similar variability between the inversion and the bottom-up model.

**Received 10 April; accepted 3 August 2006.**


1. IPCC. *Climate Change 2001: The Scientific Basis. Contribution of Working Group I to the Third Assessment Report of the Intergovernmental Panel on Climate Change* (eds Houghton, J. T. *et al.*) (Cambridge Univ. Press, Cambridge and New York, 2001).
2. Dlugokencky, E. J. *et al.* Atmospheric methane levels off: temporary pause or a new steady-state? *Geophys. Res. Lett.* **30,** 1992, doi:10.1029/2003GL018126 (2003).
3. Dentener, F. *et al.* Interannual variability and trend of $CH_4$ lifetime as a measure for OH changes in the 1979–1993 time period. *J. Geophys. Res.* **108,** 4442, doi:10.1029/2002JD002916 (2003).
4. Dlugokencky, E. J. *et al.* Changes in $CH_4$ and CO growth rates after the eruption of Mt Pinatubo and their link with changes in tropical tropospheric UV flux. *Geophys. Res. Lett.* **23,** 2761–2764 (1996).
5. Dlugokencky, E. J. *et al.* A dramatic decrease in the growth-rate of atmospheric methane in the Northern-Hemisphere during 1992. *Geophys. Res. Lett.* **21,** 507–507 (1994).
6. Langenfelds, R. L. *et al.* Interannual growth rate variations of atmospheric $CO_2$ and its δ C-13, H-2, $CH_4$, and CO between 1992 and 1999 linked to biomass burning. *Glob. Biogeochem. Cycles* **16,** 1048, doi:10.1029/2001GB001466 (2002).
7. Manning, M. R., Lowe, D. C., Moss, R. C., Bodeker, G. E. & Allan, W. Short-term variations in the oxidizing power of the atmosphere. *Nature* **436,** 1001–1004 (2005).
8. Page, S. E. *et al.* The amount of carbon released from peat and forest fires in Indonesia during 1997. *Nature* **420,** 61–65 (2002).
9. Van der Werf, G. R. *et al.* Continental-scale partitioning of fire emissions during the 1997 to 2001 El Niño/La Niña period. *Science* **303,** 73–76 (2004).
10. Walter, B. P., Heimann, M. & Matthews, E. Modeling modern methane emissions from natural wetlands 2. Interannual variations 1982–1993. *J. Geophys. Res.* **106,** 34207–34219 (2001).
11. Wang, J. S. *et al.* A 3-D model analysis of the slowdown and interannual variability in the methane growth rate from 1988 to 1997. *Glob. Biogeochem. Cycles* **18,** 3011, doi:10.1029/2003GB002180 (2004).
12. Warwick, N. J., Bekki, S., Law, K. S., Nisbet, E. G. & Pyle, J. A. The impact of meteorology on the interannual growth rate of atmospheric methane. *Geophys. Res. Lett.* **29,** 1947, doi:10.1029/2002GLO15282 (2002).
13. Chen, Y. H. & Prinn, R. G. Estimation of atmospheric methane emissions between 1996 and 2001 using a three-dimensional global chemical transport model. *J. Geophys. Res.* **111,** doi:10.1029/2005JD006058 (2006).
14. Mikaloff Fletcher, S. E. M., Tans, P. P., Bruhwiler, L. M., Miller, J. B. & Heimann, M. $CH_4$ sources estimated from atmospheric observations of $CH_4$ and its C-13/C-12 isotopic ratios: 1. Inverse modeling of source processes. *Glob. Biogeochem. Cycles* **18,** GB4004, doi:10.1029/2004GB002223 (2004).
15. Simmonds, P. G. *et al.* A burning question. Can recent growth rate anomalies in the greenhouse gases be attributed to large-scale biomass burning events? *Atmos. Environ.* **39,** 2513–2517 (2005).
16. Butler, T. M., Rayner, P. J., Simmonds, I. & Lawrence, M. G. Simultaneous mass balance inverse modeling of methane and carbon monoxide. *J. Geophys. Res.* **110,** D21310, doi:10.1029/2005JD006071 (2005).
17. Hauglustaine, D. A. *et al.* Interactive chemistry in the Laboratoire de Meteorologie Dynamique general circulation model: description and background tropospheric chemistry evaluation. *J. Geophys. Res.* **109,** D04314, doi:10.1029/2003JD003957 (2004).
18. Uppala, S. M. *et al.* The ERA-40 reanalysis. *Q. J. R. Meteorol. Soc.* **131,** 2961–3012 (2005).
19. Bousquet, P., Hauglustaine, D. A., Peylin, P., Carouge, C. & Ciais, P. Two decades of OH variability as inferred by an inversion of atmospheric transport and chemistry of methyl chloroform. *Atmos. Chem. Phys.* **5,** 2635–2656 (2005).
20. Bousquet, P. *et al.* Regional changes in carbon dioxide fluxes of land and oceans since 1980. *Science* **290,** 1342–1346 (2000).
21. Rodenbeck, C., Houweling, S., Gloor, M. & Heimann, M. $CO_2$ flux history 1982–2001 inferred from atmospheric data using a global inversion of atmospheric transport. *Atmos. Chem. Phys.* **3,** 1919–1964 (2003).
22. Keppler, F., Hamilton, J. T. G., Braβ, M. & Rockmann, T. Methane emissions from terrestrial plants under aerobic conditions. *Nature* **439,** 187–191 (2006).
23. Prigent, C., Matthews, E., Aires, F. & Rossow, W. B. Remote sensing of global wetland dynamics with multiple satellite data sets. *Geophys. Res. Lett.* **28,** 4631–4634, doi:10.1029/2001GL013263 (2001).
24. Hoerling, M. & Kumar, A. The perfect ocean for drought. *Science* **299,** 691–694 (2003).
25. Hansen, J., Ruedy, R., Sato, M. & Reynolds, R. Global surface air temperature in 1995: return to pre-Pinatubo level. *Geophys. Res. Lett.* **23,** 1665–1668 (1996).
26. Dlugokencky, E. J., Steele, L. P., Lang, P. M. & Masarie, K. A. The growth-rate and distribution of atmospheric methane. *J. Geophys. Res.* **99,** 17021–17043 (1994).

27. Bergamaschi, P. *et al.* Inverse modelling of national and European $CH_4$ emissions using the atmospheric zoom model TM5. *Atmos. Chem. Phys.* **5,** 2431–2460 (2005).
28. Gurney, K. R. *et al.* Towards robust regional estimates of $CO_2$ sources and sinks using atmospheric transport models. *Nature* **415,** 626–630 (2002).
29. GLOBALVIEW-$CH_4$. *Cooperative Atmospheric Data Integration Project—Methane* CD-ROM (NOAA/CMDL, Boulder, CO, 2005).
30. Miller, J. B. *et al.* Development of analytical methods and measurements of C-13/C-12 in atmospheric $CH_4$ from the NOAA Climate Monitoring and Diagnostics Laboratory global air sampling network. *J. Geophys. Res.* **107,** 4178, doi:10.1029/2001JD000630 (2002).
31. Quay, P. *et al.* The isotopic composition of atmospheric methane. *Glob. Biogeochem. Cycles* **13,** 445–461 (1999).
32. Tyler, S. C. *et al.* Stable carbon isotopic composition of atmospheric methane: a comparison of surface level and free tropospheric air. *J. Geophys. Res.* **104,** 13895–13910 (1999).
33. Hein, R., Crutzen, P. J. & Heimann, M. An inverse modeling approach to investigate the global atmospheric methane cycle. *Glob. Biogeochem. Cycles* **11,** 43–76 (1997).

**Supplementary Information** is linked to the online version of the paper at www.nature.com/nature.

**Acknowledgements** We thank P. Rayner, F. Chevallier and F.-M. Breon for comments on the manuscript, and P. Quay for published $\delta^{13}C$-$CH_4$ measurements for the period 1989–1995. Atmospheric $CH_4$ measurements from Réseau Aatmosphérique de Mesure des Composés à Effet de Serre (RAMCES) at Laboratoire des Sciences du Climat et de l'Environnement (LSCE) were partly funded by Institut National des Sciences de l'Univers (INSU). All calculations were realized with Commisariat à l'Energie Atomique (CEA), Centre National de la Recherche Scientifique (CNRS), Institut Pierre Simon Laplace (IPSL) and LSCE computers and support. The development of the Global Fire Emissions Dataset (GFED) used here was supported by a grant from the National Aeronautics and Space Administration (NASA).

**Author Contributions** The main contributions of each author are: P.B.: inversions, data analysis and coordination. P.C.: inverse method and manuscript improvements. J.B.M.: $CH_4$ and $\delta^{13}C$-$CH_4$ data analysis and inversion analysis. E.J.D.: $CH_4$ measurements and manuscript improvements. D.A.H.: chemistry-transport model and manuscript improvements. C.P and F.P.: satellite retrievals of flooded areas. G.R.V.d.W.: $CH_4$ emissions from fires. P.P. and C.C.: inversion method. R.L.L.: $CH_4$ measurements and manuscript improvements. E.G.B., M.R., M.S., L.P.S. and S.C.T.: $CH_4$ measurements. J.L.: plant source analysis. J.W.: $\delta^{13}C$-$CH_4$ measurements.

**Author Information** Reprints and permissions information is available at www.nature.com/reprints. The authors declare no competing financial interests. Correspondence and requests for materials should be addressed to P.B. (philippe.bousquet@cea.fr).